Atomic force microscopy and x-ray photoelectron spectroscopy investigations of the morphology and chemistry of a PdCl2/SnCl2 electroless plating catalysis system adsorbed onto shape memory alloy particles

Jean-François Silvain, Olivier Fouassier, S. Lescaux

Journal of Applied Physics

RESEARCH ARTICLE | OCTOBER 28 2004

Atomic force microscopy and x-ray photoelectron spectroscopy investigations of the morphology and chemistry of a $PdCl_2 / SnCl_2$ electroless plating catalysis system adsorbed onto shape memory alloy particles

J. F. Silvain; O. Fouassier; S. Lescaux

J. Appl. Phys. 96, 4945–4951 (2004)
https://doi.org/10.1063/1.1787625

Atomic force microscopy and x-ray photoelectron spectroscopy investigations of the morphology and chemistry of a $PdCl_2/SnCl_2$ electroless plating catalysis system adsorbed onto shape memory alloy particles

J. F. Silvain[a] and O. Fouassier
Institut de Chimie de la Matière Condensée de Bordeaux (ICMCB) - CNRS, Universite de Bordeaux 1, 87 Avenue du Dr A. Schweitzer, F-33608 PESSAC, France

S. Lescaux
Veeco, Z.I. de la Gaudrée, 11 Rue Marie Poussepin, F-91412 Dourdain, France

(Received 9 February 2004; accepted 8 July 2004)

A study of the different stages of the electroless deposition of copper on micronic NiTi shape memory alloy particles activated by one-step and two-step methods has been conducted from both a chemical and a morphological point of view. The combination of x-ray photoelectron spectroscopy (XPS) measurements and atomic force microscopy (AFM) imaging has allowed detection of the distribution of the formed compounds and depth quantification and estimation of the surface topographic parameters. For the two-step method, at the sensitization of the early stages, it is observed by AFM that Sn is absorbed in form of clusters that tend to completely cover the surface and form a continuous film. XPS analysis have shown that Sn and Pd are first absorbed in form of oxide (SnO_2 and PdO) and hydroxide $[Sn(OH)_4]$. After the entire sensitization step, the NiTi substrate is covered with Sn-based compounds. After the sensitization and the activation steps the powder roughness increases. Behavior of the Sn and Pd growth for the one-step method does not follow the behavior found for the two-step method. Indeed, XPS analysis shows a three-dimensional (3D) growth of Pd clusters on top of a mixture of metallic tin, oxide (SnO) and hydroxide $[Sn(OH)_2]$. These Pd clusters are covered with a thin layer of Pd-oxide contamination induced by the electroless process. The mean roughness for the one-step and two-step processes are equivalent. After copper deposition, the decrease of mean roughness is attributed to a filling of surface valleys, observed after the Sn-Pd coating step. © *2004 American Institute of Physics*.
[DOI: 10.1063/1.1787625]

I. INTRODUCTION

Electroless metal deposition and autocatalytic chemical processes are widely used for the growth of many metal and alloys on many surfaces. Due to its simple, low cost, and easy to use process,[1] it has been used in fields such as avionics and electronics[2] for the metallization of simple and complex metallic, ceramic[3,4] and plastic[5] substrates. This method can be used in order to obtain either thick or thin (<1 μm) uniform coatings.

Our interest in electroless metal deposition processes are related to research in the production of metal matrix composite where shape memory alloy (SMA) NiTi particles are introduced inside a liquid matrix. Due to the nonwetting properties of NiTi with the liquid SrPb matrix, a copper thin film, which has a contact angle with the liquid SnPb matrix less than 90°,[6] is electrolessly deposited on NiTi substrates.

The process we used first was essentially based on the dipping of SMA NiTi powders, at room temperature, in two successive baths. The first one was used to remove any surface oxide traces, while the second one, the coating bath, was used to coat NiTi surface with copper. However, whatever the dipping time and the bath composition, copper thin films had never before been successfully deposited on NiTi substrates.

In order to grow electroless copper on that substrate, localized catalytic centers have to be created on the NiTi surface; they will help initiate electroless metal deposition. Palladium clusters chemisorbed on the substrate surface constitute these sites. Following two main methods have been proposed: (1) the conventional two-step process which used, successively, dilute solutions of $SnCl_2$ (sensitization bath) and then $PdCl_2$ (activation bath),[7,8,9] and (2) the one-step process which used a mixed $SnCl_2$-$PdCl_2$ solutions.[7,10] The reaction should then proceed autocatalytically to form a homogeneous metal film on the surface. Extensive literature can be found on this subject,[7–9,11–13] but the reaction mechanisms and the role of the substrate are unclear. In this sense, we have investigated in details the mechanism of electroless Sn and Pd coating of NiTi smart memory alloy (SMA) with the help of atomic force microscopy (AFM), x-ray photoelectron spectroscopy (XPS) and scanning electron microscopy (SEM) for the two-step ($SnCl_2+PdCl_2$ solution) and one-step ($SnCl_2$-$PdCl_2$ mixed solution) methods. NiTi particle size measurement performed by laser granulometry shows that most of the particle size ranged 5–10 μm.

[a]Author to whom correspondence should be addressed; FAX: (33) 5 40 00 83 21; Electronic mail: silvain@icmb-bordeaux.cnrs.fr

II. EXPERIMENTAL PROCEDURES

In our experiments, the electroless process is essentially based on dipping, at room temperature, NiTi SMA powders in three (deoxidation, sensitization-activation, and coating) or four (deoxidation, sensitization, activation, and coating) different and successive baths as described previously.[6]

AFM was used in order to investigate the morphology of Sn, Sn-Pd, and Sn-Pd-Cu clusters adsorbed onto NiTi micronic particles. The Tapping Mode™ technique, using a Digital Instrument D3100 AFM, enables us to perform, at the same time, both topographic and phase imaging. In the tapping mode, the probe, which is only in intermittent contact with the sample, is rastered across the sample; the amplitude of vertical deflection of the cantilever yields topographic information.

XPS was used to investigate Sn, Pd, and Cu adsorption processes on the NiTi surface. Depth profiling by XPS was conducted using a VG ESCALAB 220 i-XL instrument, with a monochromated Al $K\alpha$ radiation source (150 μm spot diameter). In all cases, the spectra charged referenced to hydrocarbon contamination C 1*s* peak at a binding energy (BE) of 284.5 eV.

Depth profiling was achieved by argon ion etching with 3 keV ions. The measured sample current during depth profiling was 1 μA. The etched area was 3×3 mm^2 and the approximate etching rate was 0.25 nm/min. The relatively large etching area compared with that being analyzed (150 μm) ensures that experimental artifacts from the side of the sputtered area or induced roughness are minimized.[13] Also, in order to minimize any artifacts arising from different sample preparation processes, several samples were analyzed. Deconvolution of the spectra was achieved by fitting the data with a Gaussian/Lorentzian combination peak shape with variation in peak full width at half maximum, position and height being determined by an iterative program. The peak identification were determined by reference to an XPS database[14–16] or from compounds analyzed in the same apparatus.

III. RESULTS AND DISCUSSION

A. NiTi powders

The AFM analysis of as received and deoxided NiTi particles are shown in Figs. 1 and 2, respectively. The evolution of the arithmetic mean roughness (R_a) and of the maximum roughness (R_{max}) is shown in Fig. 3. For as received and deoxided powders, the observed area is 1×1 μm^2 [Fig. 1(a)] and 4×4 μm^2 [Fig. 2(a)], respectively. The evolution of the surface roughness along a single line is indicated from −2.5 to +2.5 nm for the as received powders and from −250 to +250 nm for the deoxided powders. The surface of the as received powders is apparently very smooth as pictured in Fig. 1; in contrast, deoxided powders are rougher as illustrated in Fig. 2(a) (white contrast) and in Fig. 3. From XPS analysis,[17] a schematic representation of the different oxide and carbide species on the NiTi surface (see Fig. 4), which are mainly due to the elaboration process conditions, can be proposed. It should be noted that the thickness of the three oxide and carbide top layers measured for the deoxided samples is much smaller than for the as received one but the sequence of formation is conserved. The presence of titanium carbide at the NiTi close surface can be attributed to carbon contamination, induced during the atomization process.

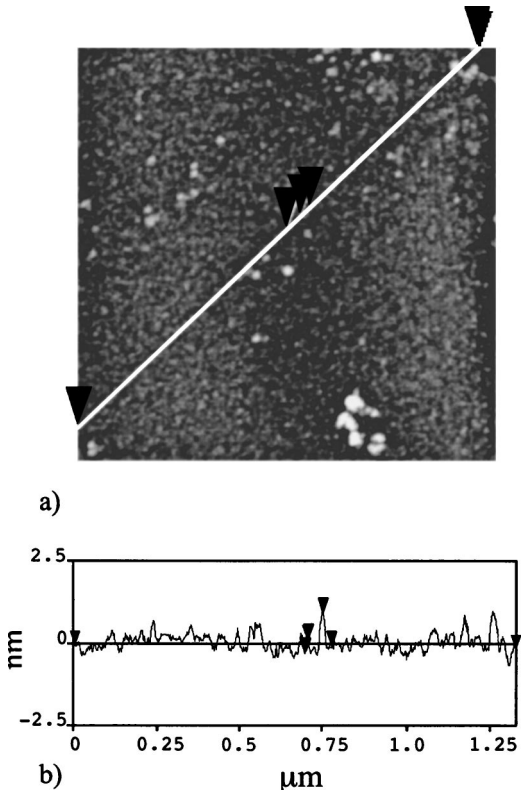

FIG. 1. (a) Surface morphology of the as received NiTi particles (1×1 μm^2). (b) Height variation obtained along the line scan shown in (a).

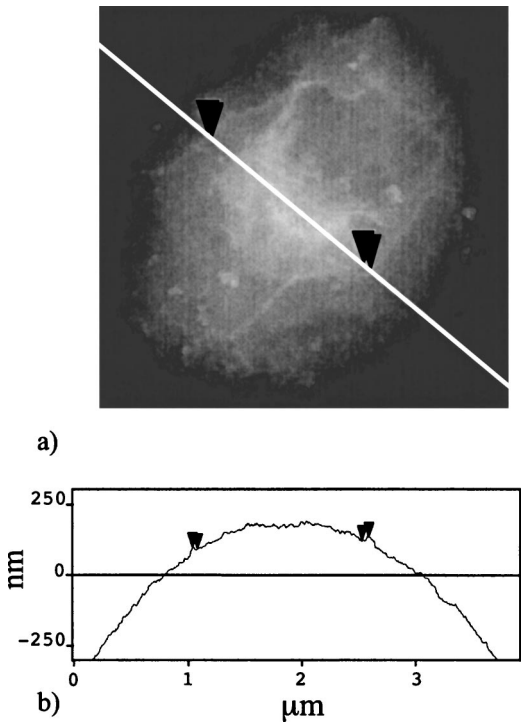

FIG. 2. (a) Surface morphology of the deoxided NiTi particles (4×4 μm^2). (b) Height variation obtained along the line scan shown in (a).

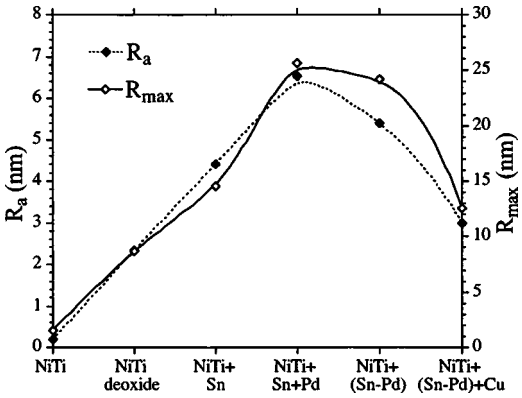

FIG. 3. Three-dimensional surface roughness obtained by AFM for various samples: R_a, the arithmetic mean roughness; R_{max}, max. − min. roughness. (1 min dipping time in different chemical bath).

B. Two-step process

1. NiT+Sn *substrate*

Samples subjected to short Sn deposition times (several seconds) have been initially selected for XPS analysis. In order to understand how Sn atoms interact with the NiTi substrate, the XPS results before and during Ar^+ sputtering are discussed. All values are presented in Table I. The decomposition of the O 1*s* peak shows three components: one at low BE (529.6 eV) attributed to TiO_2 oxide, and two at higher BE (531.58 eV and 532.96 eV) characteristic of other metal-oxide and C═O species. It should be noted that all carbon peaks, located between 284.5 and 288.2 eV, which are assigned to C—C, C—O, and C═O, respectively, disappear after the first run of sputtering in all samples studied. Consequently, the contribution of oxygen and carbon will be neglected in further discussions.

As for the NiTi surface, the Ti 2*p* peak can be decomposed in three components (cf. Table I): one characteristic of NiTi bonds and the two others of Ti oxides, which do not vanish when analyzing inner layers. The evolution, with Ar^+ sputtering time, of the titanium oxide binding energies, is mainly due to a preferential oxygen removal effect.[18] Indeed, after Ar^+ sputtering (of TiO_2 and Ti_2O_3), TiO_x surface, with BE ranging from 456 to 458 eV, are formed. The presence of the titanium species indicates that, after several seconds of immersion, the NiTi is still detected at the sample surface.

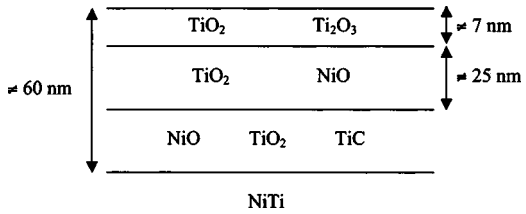

FIG. 4. Schematic illustration, obtained after XPS analysis, of the NiTi surface.

Before Ar^+ sputtering, the Sn peak needed to be characterized by two contributions. The higher one, at 487.40 eV, corresponds to oxides (SnO_2) and chloride ($SnCl_2$) species. The lower BE one, at 485.5 eV, is assigned to metallic Sn (Sn^0). A small peak corresponding to Cl $2p_{3/2}$ at 198.4 and 199.7 eV, assigned respectively to $SnCl_2$ and/or Cl—C—O, is also present on the surface but vanishes after short sputtering times. Since also the Sn components corresponding to SnO_2 vanish after short sputtering times, it is concluded that the $SnCl_2$ and the Sn oxide are only present at the surface and that, at depth greater than 15 nm, the deposit is essentially composed of Sn. Also, catalysis sites of the NiTi surface are covered by pure tin metal (XPS results for long sputtering time).

From the above discussion, it can be concluded that Sn atoms are first absorbed on the NiTi substrate in metal forms (Sn^0), through the possible reactions,

$$Sn^{2+} + Ti \rightarrow Ti^{2+} + Sn$$

The samples subjected to short Sn depositions times have also provided significant information about the evolution of the Sn nucleation sites on NiTi. Figure 5(a) shows AFM top-view phase images ($4 \times 4\ \mu m^2$) and the evolution of the surface roughness along a single line is indicated from −250 nm to 250 nm [Fig. 5(b)]. It is observed that, after deposition, the NiTi surface appears covered of isolated Sn clusters (cf. Fig. 5) of 50–100 nm average diameter. Figure 3 directly infers that the surface area of the treated NiTi surface, whatever the surface treatment, is much wider than that on the deoxidized NiTi one. In addition, the surface area increases with dipping time in the chemical bath and with the number of chemical bath used for the each process. The cluster size at these early stages do not change appreciably with

TABLE I. Cl $2p_{3/2}$, Sn $3d_{5/2}$, Ti $2p_{3/2}$, and Ni $2p_{3/2}$ BEs, before and after Ar^+ sputtering of NiTi+Sn materials; BE (eV) [FWHM (eV)] **Area** (%) Attributed species (two-step process: NiTi+Sn substrate).

Argon sputtering	Cl $2p_{3/2}$	Sn $3d_{5/2}$	Ti $2p_{3/2}$	Ni $2p_{3/2}$
0 s	198.3 (1.4) **48** $SnCl_2$	485.5 (1.2) **15** Sn	454.5 (1.2) **3** NiTi	
	199.7 (1.4) **52** Cl—O—C	487.4 (2.1) **85** $SnO_2 \cdot 2H_2O$	456.4 (1.4) **11** Ti_2O_3	
		$SnCl_2$	458.9 (1.8) **86** TiO_2	
180 s (15 nm)		485.4 (1.2) **43** Sn	454.9 (1.1) **17** NiTi	853.4 (1.1) NiTi
		487.4 (2.0) **57** $SnO_2 \cdot 2H_2O$	455.9 (1.1) **18** Ti_2O_3	
			457.0 (1.4) **9** TiO_x	
			459.3 (1.7) **36** TiO_2	
1000 s (80 nm)		485.2 (1.3) Sn	454.7 (1.0) **54** NiTi	853.4 (1.2) NiTi
			455.6 (1.0) **24** TiO_x	
			456.5 (1.4) **16** TiO_x	
			457.7 (1.7) **6** TiO_x	

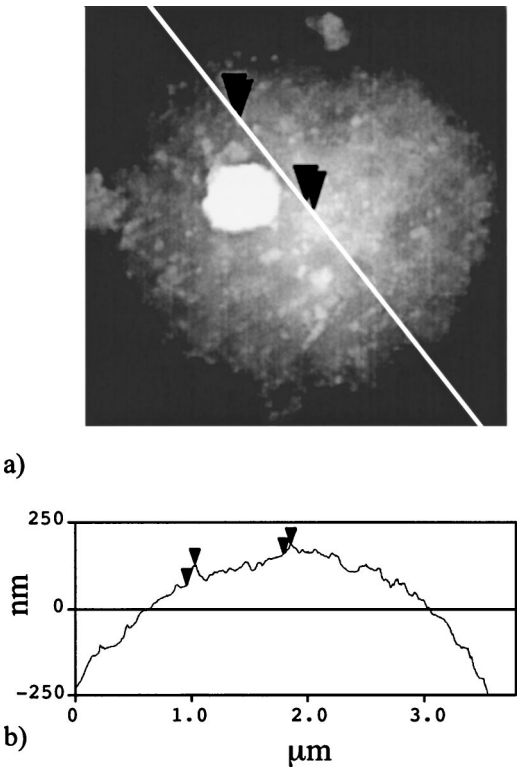

FIG. 5. (a) Surface morphology of the NiTi+Sn particles (4×4 μm^2). (b) Height variation obtained along the line scan shown in (a).

immersion time and the presence of agglomerates is hardly observed, which indicates that Sn deposition on NiTi starts as a 3D process, and that the coalescence of the individual clusters gives rise to a continuous layer and, therefore, to a 2D growth.

2. NiTi+Sn+Pd *powders*

Table II shows the typical evolution, after peak decomposition, of the NiTi+Sn+Pd surface. Before and after Ar^+ sputtering, Ti, Ni, Sn, Pd, O, and C signals are detected on all samples; therefore, the various components of the Ti $2p_{3/2}$, Ni $2p_{3/2}$, Sn $3d_{5/2}$, Pd $3d_{5/2}$, and O 1*s* XPS peaks have been extracted. The decomposition of the Ti $2p_{3/2}$, Ni $2p_{3/2}$, and O 1*s* peaks, which are, in fact, almost similar to the NiTi+Sn samples (cf. Table I), will not be discussed. On the other hand, evolution of the Pd and Sn species before and after Ar^+ sputtering is analyzed.

Before Ar^+ sputtering and for short sputtering time, the Sn BE peak presents four main contributions (cf. Table II). Two of them correspond to Sn hydroxide [$SnO_2\cdot2H_2O$ or $Sn(OH)_4$] and oxide (SnO_2), another to metallic Sn, and a small contribution, at 489.0 eV, that is unclear (the nearest peak reported in the literature, at 487.4 eV, is assigned to $SnCl_2\cdot2H_2O$). The Sn^0 state at 485.3 eV, which is $\approx$1 eV higher than the corresponding BE for pure Sn metal, may be assigned to a Sn-Pd alloy system. The Sn metal contributions decrease with argon sputtering time, and only the contributions of the Sn oxides remain after 1000 s of argon bombardment.

Finally, the BE peak of Pd was fitted using two components: the highest energy one, at 336.2 eV, is attributed to PdO and/or Pd-Sn alloy; the lower energy one, at 334.6 eV, is attributed to pure metallic Pd. The higher BE contribution increases with increasing Ar^+ sputtering time, while the Pd^0 disappears after long ion-bombardment time.

Taking into account the above results for the NiTi+Sn and NiTi+Sn+Pd systems, the possible mechanisms of Sn adsorption and Pd absorption are proposed. For the NiTi+Sn system, XPS results show that Sn is absorbed in the form of Sn^0, where Sn atoms do not react with the O^{2-} ions of the Ti and Ni oxides. In addition, no clear proof of chemical reactions between Ni and/or Ti atoms with the Sn ones has been determined by the XPS. On the other hand, after the Pd bath, XPS results show that Sn^{4+} states are now present at the NiTi surface. Therefore, it can be concluded that, inside the palladium bath, Sn atoms react with the $PdCl_2$ species to form Pd^0, which can then react with the NiTi oxides to form Pd and Sn oxide species via O^{2-} ions.

Figure 6(a) shows an AFM topographic image (4×4 μm^2) corresponding to 30 s of immersion time in the $PdCl_2$ bath. Figures 3 and 6(b) clearly show that surface roughness and the area increase in comparison with the NiTi+Sn surface. The increase of the 3D surface roughness may be ascribed to Sn re-dissolution into the Pd bath, to Pd growth habits (presence of high peaks), or to both effects.

TABLE II. Sn $3d_{5/2}$, Pd $3d_{5/2}$, Ti $2p_{3/2}$, and Ni $2p_{3/2}$ BEs, before and after Ar^+ sputtering of NiTi+Sn+Pd materials; BE (eV) [FWHM (eV)] **Area** (%) Attributed species (two-step process: NiTi+Sn+Pd substrate).

Argon sputtering	Sn $3d_{5/2}$	Pd $3d_{5/2}$	Ti $2p_{3/2}$	Ni $2p_{3/2}$
0 s	485.3 (1.1) **52** Sn-Pd	334.6 (1.9) **40** Pd	454.8 (1.1) **5** NiTi	
	487.2 (1.5) **33** $SnO_2\cdot2H_2O$	336.2 (1.9) **60** PdO	455.9 (1.5) **10** Ti_2O_3	
	487.9 (1.6) **4** SnO_2	Pd-Sn	459.6 (1.8) **85** TiO_2	
	489.0 (1.6) **11** ?			
180 s (15 nm)	485.3 (1.1) **25** Sn-Pd	334.6 (1.9) **20** Pd	454.8 (1.1) **28** NiTi	853.4 (1.1) **84** NiTi
	487.2 (1.5) **45** $SnO_2\cdot2H_2O$	336.2 (1.9) **80** PdO	455.9 (1.5) **22** Ti_2O_3	854.7 (2.5) **16** NiO
	487.9 (1.6) **25** SnO_2	Pd-Sn	457.0 (1.4) **16** TiO_x	
	489.0 (1.6) **5** ?		459.6 (1.8) **34** TiO_2	
1000 s (80 nm)	487.2 (1.5) **35** $SnO_2\cdot2H_2O$	336.2 (1.9) PdO	454.7 (1.1) **40** NiTi	853.4 (1.2) **90** NiTi
	487.9 (1.6) **65** SnO_2		455.9 (1.5) **26** TiO_x	854.7 (2.5) **10** NiO
			457.0 (1.4) **17** TiO_x	
			459.6 (1.8) **17** TiO_2	

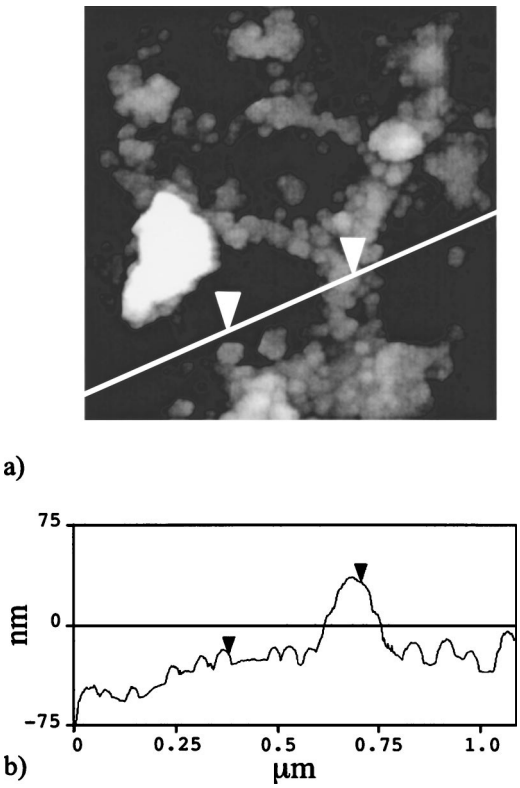

FIG. 6. (a) Surface morphology of the NiTi+Sn+Pd particles (4×4 μm^2). (b) Height variation obtained along the line scan shown in (a).

Taking into account XPS and AFM results, a schematic representation of the different tin and palladium species present on the NiTi surface is proposed [cf. Fig. 7(a)] for the two-step electroless process.

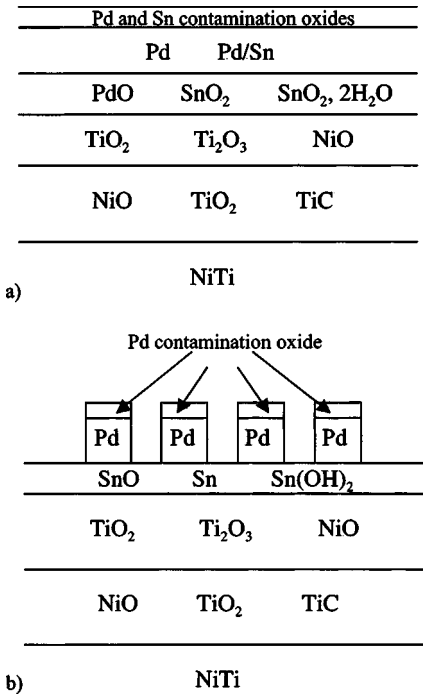

FIG. 7. Schematic illustration, obtained after AFM and XPS analysis, of (a) the NiTi+Sn+Pd surface and (b) the NiTi+(Sn-Pd) surface.

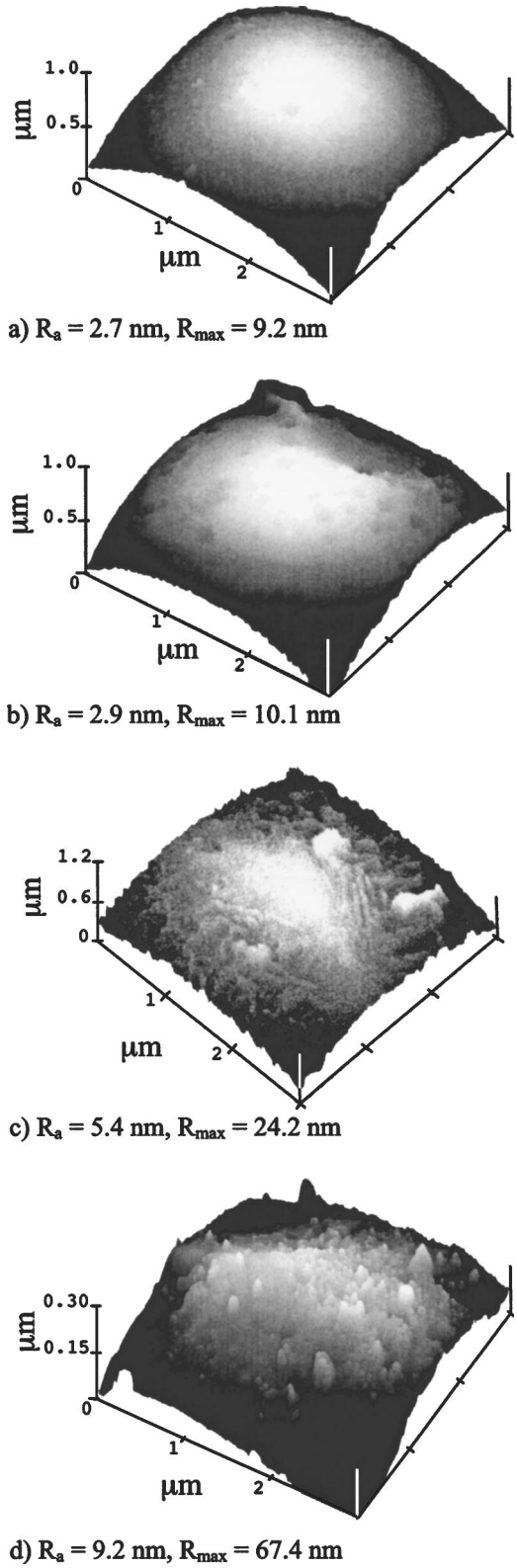

FIG. 8. Evolution of the surface morphology of the NiTi particles after different immersion time in the mixed (Sn-Pd) bath: (a) 10 s, (b) 30 s, (c) 1 min, and (d) 10 min (R_a, the arithmetic mean roughness; R_{max}, max.−min. roughness).

3. One-step process

Table III shows the typical evolution, after peak decomposition, of the NiTi+(Sn−Pd) surface. Before and after Ar^+ sputtering, Ti, Ni, Sn, Pd, O, and C signals are detected on

TABLE III. Sn $3d_{5/2}$, Pd $3d_{5/2}$, Ti $2p_{3/2}$, and Ni $2p_{3/2}$ BEs, before and after Ar^+ sputtering of NiTi+Sn-Pd materials; BE (eV) [FWHM (eV)] **Area** (%) Attributed species [one-step process: NiTi+(Sn-Pd) substrate].

Argon sputtering	Sn $3d_{5/2}$	Pd $3d_{5/2}$	Ti $2p_{3/2}$	Ni $2p_{3/2}$
0 s	486.6 (1.6) **80** $SnO,Sn(OH)_2$	335.3 (1.5) **66** Pd	458.3 (1.4) **60** Ti_2O_3	
	488.6 (1.6) **20** ?	337.1 (1.4) **34** PdO	459.9 (1.7) **40** TiO_2	
60 s (5 nm)	484.5 (1.4) **20** Sn	335.6 (1.4) Pd	453.8 (1.1) **25** Ti	852.2 (1.1) **80** NiTi
	486.4 (1.6) **55** SnO		454.8 (1.1) **30** NiTi	853.7 (1.5) **20** NiO
	488.6 (1.6) **25** ?		458.2 (1.4) **28** TiO_x	
			459.7 (1.5) **17** TiO_2	
180 s (15 nm)	484.2 (1.2) **60** Sn	335.2 (1.9) Pd	453.8 (1.2) **70** Ti	852.2 (1.0) **95** NiTi
	486.3 (1.4) **40** SnO		455.2 (1.3) **20** NiTi	853.7 (1.6) **5** NiO
			459.8 (1.5) **10** TiO_2	

all samples. The decomposition of the Ti $2p_{3/2}$, Ni $2p_{3/2}$, and O 1*s* peaks, which are, in fact, almost similar to the NiTi+Sn+Pd samples (cf. Table II), will not be discussed. On the other hand, the evolution of the Sn and Pd before and after Ar^+ sputtering is analyzed.

Before and after Ar^+ sputtering, the Sn 3*d* doublet envelope is complex and can be associated, after curve-fitting, with the presence of two (surface and long Ar^+ sputtering time) or three chemically distinct species (cf. Table III). The peak positions resulting from this procedure are 484.5, 486.4, and 488.6 eV, corresponding to Sn^0, Sn^{2+}, and $Sn^?$ oxidation states, respectively. The low BE peak can be easily assigned to the pure Sn metal (Sn^0) and the middle BE peak is attributed to SnO or $Sn(OH)_2$(Sn^{2+}). Since there is no evidence for a Cl peak from XPS, it is unlikely that the Sn^{2+} species is produced by residual $SnCl_2$ on the substrate surface. As for the NiTi+Sn+Pd system, the remaining line, in terms of the observed BE, has no clear correspondence.

Before Ar^+ sputtering, two components—one at lowest BE (335.3 eV) assigned to metallic Pd (Pd^0) and one at highest BE (337.1 eV) assigned to palladium oxide (PdO)—have been detected. In contrast to the two-step method, where Pd 3*d* BE at 336.2 eV (Pd-Sn alloy system) is associated with Sn 3*d* BE at 485.3 eV (Sn-Pd alloy system), the metal BE peak of Sn (484.5 eV) cannot be associated with any Sn-Pd alloy system. Therefore, the Pd metal BE which is $\approx$1 eV higher than the corresponding BE for pure Pd, may be assigned to a nanometric cluster shape. In this sense, Fristch *et al.*,[19] Nosova *et al.*,[20] and Voogt *et al.*,[21] show that the shape difference between a Pd metallic (Pd^0) film and nanometric metallic Pd (Pd^0) clusters can be associated with an increase of the Pd $3d_{5/2}$ BE. For these authors, the BE change is mainly related to the reduction of the cluster valence electrons or by relaxation effect which tends, in both explanations, to increase the BE when the cluster size decreases. Conversely, short Ar^+ sputtering time leads to a complete removal of the palladium oxide species, which therefore can be attributed to normal surface oxidation phenomena, induced after the electroless Pd deposition. A schematic representation of the different titanium, nickel, tin and palladium species present on the NiTi surface is proposed [cf. Fig. 7(b)] for the one-step electroless process.

The evolution of the arithmetic mean roughness and of the max./min. roughness parameters along the Pd deposition are displayed in Fig. 8. It can be observed that both values sharply increase after deposition time, which indicates (1) that the NiTi flatness is lost and (2) that the surface roughness increases with dipping time. This increase may be ascribed to Sn re-dissolution into the Sn-Pd bath, to Pd growth habits (presence of high peaks) or to both effects. Figure 3 shows that the 3D surface roughness data obtained for the NiTi+Sn+Pd and NiTi+(Sn-Pd) samples are quite similar. Finally, the mean roughness of the Sn-Pd/NiTi substrate, ready for Cu deposition, is R_a=6 nm, 30 times higher than that of the raw NiTi. However, from Fig. 3, a significant decrease of these values after covered-to-eye Cu indicates that the surface height differences are smaller; this decrease can be attributed to the filling of valleys by Cu.

IV. SUMMARY AND CONCLUSIONS

The different stages of the electroless deposition of copper on NiTi micronic particles activated by one-step and two-step methods have been studied by XPS and AFM. Conventional one-step and two-step processes, where dilute solutions of $SnCl_2$-$PdCl_2$ and $SnCl_2$ and $PdCl_2$ are used to promote the nucleation and growth of Cu thin films.

For the two-step method, at the sensitive early stages, it is observed that Sn is absorbed in the form of clusters that tend to completely cover the surface, thereby forming a continuous film. It has been found that Sn and Pd are initially absorbed in the form of oxide (SnO_2 and PdO) and hydroxide [$Sn(OH)_4$]. After completion of the sensitization step, the NiTi-substrate is covered with Sn-based compounds and the roughness of the Sn/NiTi substrate becomes greater than that of the raw NiTi powder. During activation, the 3D surface roughness increases, as demonstrated by AFM. The mean roughness of the Pd/Sn/NiTi substrate prior to Cu deposition is 1.5 times greater than that of the Sn/NiTi substrate. This increase is associated with the growth of Pd and Pd-Sn compounds, as verified by XPS.

Behavior of Sn and Pd growth for the one-step method does not follow the behavior found for the two-step method. Indeed, XPS analysis show a 3D growth of Pd clusters on top of a mixture of tin metal: oxide (SnO) and hydroxide [$Sn(OH)_2$]. These Pd clusters are covered with a thin layer of Pd oxide contamination induced by the electroless process. The mean roughness for the two-step and one-step processes

is equivalent. After Cu deposition, the decrease of the mean roughness is attributed to a filling of the surface valleys observed after the Sn-Pd coating.

ACKNOWLEDGMENT

The authors thank the European Community (Contract No. BRPR-CT98-0683) for supporting this project and Memry Europ for providing the Ni-Ti particles.

[1]G. O. Malloroy and J. B. Hajdu, Editors, Electrolessplating: Fundamentals and Applications, AESFS, Orlando, FL (1990).
[2]R. H. Keene, Plat. Surf. Finish. **68**, 22 (1988).
[3]S. G. Warrier, R. Y. Lin, and J. Mat, Science **28**, 4868 (1993).
[4]H. M. Cheng, B. L. Zhou, Z. G. Zheng, Z. M. Wang, and C. X. Shi, Plat. Surf. Finish. **77**, 130 (1990).
[5]M. Charbonnier, M. Alami, and M. Romand, J. Appl. Electrochem. **28**, 449 (1998).
[6]S. Trombert, J. Chazelas, M. Lahaye, and J. F. Silvain, Compos. Interfaces **5**, 479 (1998).
[7]R. L. Meek, J. Electrochem. Soc. **122**, 1478 (1975).
[8]B. K. W. Baylis, A. Busuttil, N. E. Hedgecock, and M. Schlesinger, J. Electrochem. Soc. **123**, 348 (1976).
[9]I. Kiflawick and M. Schlesinger, J. Electrochem. Soc. **130**, 872 (1983).
[10]M. Tsukahara, J. Met. Finish. Soc. Jpn. **23**, 83 (1972).
[11]T. Osaka, H. Takematsu, and K. Nihei, J. Electrochem. Soc. **127**, 349 (1977).
[12]T. Hamada, Y. Kumagai, N. Koshizaki, and T. Kanbe, Chem. Lett. **58**, 1461 (1989).
[13]S. Shukla, S. Seal, J. Akesson, R. Oder, R. Carter, and Z. Ralman, Appl. Surf. Sci. **181**, 35 (2001).
[14]N. Laegrid and G. K. Wekner, J. Appl. Phys. **32**, 365 (1961).
[15]D. Briggs and M. P. Seah, *Practical Surface Analysis* Vol. 1, AES and XPS (Wiley, New York, 1990).
[16]J. F. Moulder, W. F. Stickle, P. E. Sobol, and K. D. Bomben, *Handbook of x-ray Photoelectron Spectroscopy* (Perkin-Elmer, Eden Prairie, MN, 1992).
[17]Olivier Fouassier, PhD thesis, Bordeaux 1, No. 2401, France, 2001.
[18]J. P. Espinos, A. Fernandez, and A. R. Gonzales-Elipe, Surf. Sci. **295**, 402 (1993).
[19]A. Fritsch and P. Legare, Surf. Sci. **161**, 742 (1985).
[20]L. V. Nosova, M. V. Stenin, Yu. N. Nogin, and Yu. A. Ryndin, Appl. Surf. Sci. **55** 43 (1992).
[21]E. H. Voogt, A. J. M. Mens, O. L. J. Gijzeman, and J. W. Geus, Surf. Sci. **350**, 21 (1996).